

# A Search for Interstellar Pyrimidine

Yi-Jehng Kuan,<sup>1,2\*</sup> Chi-Hung Yan,<sup>1</sup> Steven B. Charnley,<sup>3</sup> Zbigniew Kisiel,<sup>4</sup>  
Pascale Ehrenfreund<sup>5</sup> and Hui-Chun Huang<sup>1</sup>

<sup>1</sup>*Department of Earth Sciences, National Taiwan Normal University, Taipei 116, Taiwan, ROC*

<sup>2</sup>*Institute of Astronomy and Astrophysics, Academia Sinica, P.O. Box 23-141, Taipei 106, Taiwan, ROC*

<sup>3</sup>*Space Science Division, NASA Ames Research Centre, MS 245-3, Moffett Field, CA 94035, USA*

<sup>4</sup>*Institute of Physics, Polish Academy of Sciences, Al.Lotnikow 32/46, 02-668 Warsaw, Poland*

<sup>5</sup>*Leiden Observatory, P.O. Box 9513, 2300 RA Leiden, The Netherlands*

Accepted 2003 June 30. Received 2003 June 17; in original form 2003 April 14

## ABSTRACT

We have searched three hot molecular cores for submillimeter emission from the nucleic acid building-block pyrimidine. We obtain upper limits to the total pyrimidine (beam-averaged) column densities towards Sgr B2(N), Orion KL and W51 e1/e2 of  $1.7 \times 10^{14} \text{cm}^{-2}$ ,  $2.4 \times 10^{14} \text{cm}^{-2}$  and  $3.4 \times 10^{14} \text{cm}^{-2}$ , respectively. The associated upper limits to the pyrimidine fractional abundances lie in the range  $(0.3 - 3) \times 10^{-10}$ . Implications of this result for interstellar organic chemistry, and for the prospects of detecting nitrogen heterocycles in general, are briefly discussed.

**Key words:** astrobiology – ISM: individual (Orion KL, Sgr B2(N), W51 e1/e2) – ISM: molecules – line: identification.

## 1 INTRODUCTION

Molecular clouds contain many organic molecules that are known to be important in biochemistry. Astronomical observations, particularly at radio wavelengths, allow us to determine the chemical composition and characteristics of this molecular inventory (e.g. Dickens et al. 2001; Charnley, Ehrenfreund & Kuan 2001). Following incorporation into protostellar disks and comets, these molecules, or their descendants, were probably the major source of volatile organic material available to the early Earth (Chyba et al. 1990). Studies of molecular cloud composition therefore enable us to quantitatively address the issue of the connection between interstellar chemistry, the organic composition of primitive Solar System material, and the origin, evolution and distribution of Life in the Galaxy (e.g. Ehrenfreund & Charnley 2000; Ehrenfreund et al. 2002).

Many organics that are known, or strongly suspected, to be present in interstellar clouds, are fundamental components of the large organic macromolecules that are central to biochemistry. Examples of these are sugars and amino acids, the respective building blocks of polysaccharides and proteins. The simplest of these, glycolaldehyde and glycine, are both identified in the interstellar medium (Hollis et al. 2000; Kuan et al. 2003a).

Until recently, definitive detections of interstellar

ring compounds have been scarce (e.g. ethylene oxide, Dickens et al. 1997) and previous searches for imidazole, cyanoforn, pyrrole and pyrimidine were unsuccessful (Simon & Simon 1973; Myers, Thaddeus & Linke 1980; Irvine et al. 1981). Recently we have tentatively detected the azaheterocyclic compounds 2H-azirine (*c*-C<sub>2</sub>H<sub>3</sub>N) and aziridine (*c*-C<sub>2</sub>H<sub>5</sub>N) at mm wavelengths (Kuan et al. 2003b; Charnley, Ehrenfreund & Kuan 2001). Two (different) tentative lines of Aziridine have also been claimed by Dickens et al. (2001). These observations suggest that biochemically important ring molecules may await detection. Of these potential discoveries, a key interstellar molecule for Astrobiology, comparable in importance to glycine, would be pyrimidine (*c*-C<sub>4</sub>H<sub>4</sub>N<sub>2</sub>), the unsubstituted ring analogue for three of the DNA and RNA bases: thymine, cytosine and uracil. Interstellar pyrimidine was unsuccessfully searched for at 46 GHz 30 years ago (Simon & Simon 1973). Evidence for various purines and pyrimidines in space, including pyrimidine, comes from the fact that they have been detected in meteoritic organic matter (Stoks & Schwartz 1981, 1982), and also may be components of Comet Halley's CHON dust (Krueger, Korth & Kissel 1991).

The molecular composition of hot molecular cores is known to largely reflect the solid state chemistry that occurred on grain surfaces, prior to their deposition into the gas after protostellar dust heating (see Ehrenfreund & Charnley 2000). Reactions between HCN and V<sub>2</sub>CN (CH<sub>2</sub>CHCN) on the surface of dust grains has been suggested as a possible source of interstellar pyrimidine (Simon & Simon 1973). Observations of hot cores,

\* E-mail: kuan@sgrb2.geos.ntnu.edu.tw (YJK)

**Table 1.** Source List

Source	R.A.(B1950)	Dec(B1950)	$V_{\text{LSR}}$ ( $\text{km s}^{-1}$ )
Orion KL	05 <sup>h</sup> 32 <sup>m</sup> 47 <sup>s</sup> .00	−05° 24′ 30″.0	8.0
Sgr B2(N)	17 <sup>h</sup> 44 <sup>m</sup> 10 <sup>s</sup> .20	−28° 21′ 15″.0	64.0
W51 e1/e2	19 <sup>h</sup> 21 <sup>m</sup> 26 <sup>s</sup> .30	+14° 24′ 39″.0	60.0

known to contain other rings believed to have formed on dust prior to evaporation, such as *c*-C<sub>2</sub>H<sub>4</sub>O (ethylene oxide) (Dickens et al. 1997; Nummelin et al. 1998) and *c*-C<sub>2</sub>H<sub>3</sub>N (Charnley, Ehrenfreund & Kuan 2001), do show the very high abundances of the HCN and VyCN molecules required for formation of N-heterocycles (Ziurys & Turner 1986; Turner 1991; Nummelin & Bergman 1999). Alternatively, experiments indicate that energetic processing of ices (e.g. Allamandola, Bernstein & Sandford 1997) leads to an organic residue containing many polycyclic aromatic hydrocarbons (PAHs) (Greenberg et al. 2000). One may speculate that similar processing of interstellar ice analogues containing ammonia, molecular nitrogen, and hydrogen cyanide, may similarly produce N-heterocycles like pyrimidine.

Hence, searches of hot molecular cores, employing high-quality spectroscopic data, may offer the best chance of a pyrimidine detection. In this paper we report the results of a search towards three massive star-forming regions for submillimeter emission from pyrimidine.

## 2 OBSERVATIONS

We carried out a program of submillimeter observations using the James Clerk Maxwell Telescope (JCMT)<sup>1</sup> on Mauna Kea, Hawaii during Semester 01B over the period September 9–13, 2001. Additional measurements were made on November 23, December 1–2, and December 10, 2001. Our target list is given in Table 1; Column 4 gives the nominal LSR velocity of each source adopted for the search. The source list consists of three well-studied regions of massive star formation which are known to be rich in complex organic molecules (e.g. Blake et al. 1987; Miao et al. 1995; Remijan et al. 2002).

The heterodyne receivers used were the dual-channel B3 SIS mixers in the single-sideband mode (SSB) for the 345 GHz submillimeter band (315–373 GHz). The sideband rejection was  $\sim 13$  dB (a factor of  $\sim 20$ ). The SSB system temperatures in fair (medium) weather conditions – atmospheric opacity  $\tau$ (225 GHz) between 0.08 and 0.12 – were generally  $\sim 400$  to 550 K. At 329.9 and 363.1 GHz, however,  $T_{\text{sys}}$  as high as  $\sim 700$  K and  $\sim 900$  K were recorded, due to poor atmospheric transmission and higher receiver temperature. The half-power beamwidth (HPBW) of the telescope is  $\sim 14''$  and the main-beam efficiency,  $\eta_{\text{mb}}$ , is 0.63. Data were obtained in the position-switching mode with offset 20' west

in azimuth. Pointing and focus was checked regularly at a 2-hour interval. The resultant spectra are on the antenna temperature scale,  $T_{\text{A}}^*$ , which has been corrected from chopper wheels calibration for atmospheric transmission and losses associated with rearward scattering. Since the spatial extent of each emission source is not known, no main beam correction is applied. Further corrections for the forward scattering and spillover efficiency ( $\eta_{\text{fss}} = 0.82$ ) convert the source antenna temperature,  $T_{\text{A}}^*$ , to the source brightness temperature,  $T_{\text{R}}^*$ .

By employing the Dutch Autocorrelation Spectrometer (DAS) backend with two subsystems and a bandwidth of 500 MHz for dual-polarity operation, we have a spectral resolution of 756 kHz and a channel spacing of 625 kHz. Typically an integration time of 3 to 4 hours was achieved. Velocity shifting of  $\pm 4.5 \text{ km s}^{-1}$  with respect to the nominal LSR velocity, about  $\pm 5$  MHz with respect to the rest frequency in the 345 GHz band, was executed as a common practice during observations in order to neutralize the effect of possible low-level gain variations in the DAS and to identify potential interlopers from the image sideband. The JCMT data were reduced using the SPECX spectral line reduction package.

Observations of submillimeter high-frequency transitions yield smaller telescope beams, preferentially sample the warmer and denser regions, and help to avoid line confusion with interloping emission from cooler envelope material along the line-of-sight. At hot core temperatures of 100 K or more, searches in the submillimeter regime are further favoured by the fact that the higher frequency transitions are expected to be intrinsically stronger.

Good agreement between observed line frequencies and those measured in the laboratory, for four or more spectral lines, are the minimum requirements for claiming identification of a new interstellar molecule. The rotational spectrum of pyrimidine has recently been measured over the spectral range 3–337 GHz, and the calculated dipole moment of pyrimidine is  $\mu_{\text{tot}} = \mu_b = 2.39$  Debye (Kisiel et al. 1999). Hence only *b*-type transitions are observable. Our astronomical search was based on the best candidate transitions of pyrimidine in spectral regions free from known spectral line contamination. Four bandheads made up of closely spaced high-*J* transitions (at higher energy levels) plus 2 pairs of low-*J* doublet lines were observed in a total of 6 different spectral bands. The observed transitions are listed in Table 2; transitions with line strengths smaller than 10.0 are not included. Column 1 lists the *line* number; each *line* may include multiple pyrimidine transitions which are blended into one unresolved, single spectral-line feature.

Figure 1 illustrates the predicted relative line intensity in an arbitrary scale of the pyrimidine spectra over a frequency range of 0 to 500 GHz at various rotational temperatures ( $T_{\text{rot}} = 50$  K, the top panel; 100 K, the middle panel; and 200 K, the bottom panel). All possible spectral blends are accounted for in the simulation, which is made for a Gaussian lineshape with an assumed equivalent linewidth (FWHM) of  $7 \text{ km s}^{-1}$ . Note that the linewidth, when Doppler converted from velocity to frequency, increases with frequency, which is conducive to the formation of stronger blends at higher frequencies.

<sup>1</sup> The JCMT is operated by the Joint Astronomy Centre in Hilo, Hawaii on behalf of the present organizations: the Particle Physics and Astronomy Research Council in the United Kingdom, The National Research Council of Canada and the Netherlands Organization for Scientific Research

**Table 2.** Pyrimidine transitions observed.

Line	Rest Frequency (MHz)	Transition $J_{K_a, K_c} - J_{K'_a, K'_c}$	$S_{ul}^*$	$E_l^\dagger$ ( $\text{cm}^{-1}$ )
1	329961.004	53 <sub>1,53</sub> - 52 <sub>0,52</sub>	52.48	288.87
	329961.004	53 <sub>0,53</sub> - 52 <sub>1,52</sub>	52.48	288.87
	329963.042	52 <sub>2,51</sub> - 51 <sub>1,50</sub>	50.45	288.46
	329963.042	52 <sub>1,51</sub> - 51 <sub>2,50</sub>	50.45	288.46
	329963.507	43 <sub>11,33</sub> - 42 <sub>10,32</sub>	32.73	266.24
	329963.507	43 <sub>10,33</sub> - 42 <sub>11,32</sub>	32.73	266.24
	329963.584	42 <sub>12,31</sub> - 41 <sub>11,30</sub>	30.83	261.71
	329963.584	42 <sub>11,31</sub> - 41 <sub>12,30</sub>	30.83	261.71
	329963.825	44 <sub>10,35</sub> - 43 <sub>9,34</sub>	34.65	270.36
	329963.825	44 <sub>9,35</sub> - 43 <sub>10,34</sub>	34.65	270.36
	329964.312	41 <sub>12,29</sub> - 40 <sub>13,28</sub>	28.95	256.77
	329964.312	41 <sub>13,29</sub> - 40 <sub>12,28</sub>	28.95	256.77
	329964.345	45 <sub>9,37</sub> - 44 <sub>8,36</sub>	36.58	274.06
	329964.345	45 <sub>8,37</sub> - 44 <sub>9,36</sub>	36.58	274.06
	329964.448	51 <sub>3,49</sub> - 50 <sub>2,48</sub>	48.43	287.64
	329964.448	51 <sub>2,49</sub> - 50 <sub>3,48</sub>	48.43	287.64
	329964.911	46 <sub>8,39</sub> - 45 <sub>7,38</sub>	38.52	277.36
	329964.911	46 <sub>7,39</sub> - 45 <sub>8,38</sub>	38.52	277.36
	329965.303	50 <sub>3,47</sub> - 49 <sub>4,46</sub>	46.43	286.41
	329965.303	50 <sub>4,47</sub> - 49 <sub>3,46</sub>	46.43	286.41
	329965.396	47 <sub>7,41</sub> - 46 <sub>6,40</sub>	40.48	280.24
	329965.396	47 <sub>6,41</sub> - 46 <sub>7,40</sub>	40.48	280.24
	329965.687	49 <sub>4,45</sub> - 48 <sub>5,44</sub>	44.43	284.76
	329965.687	49 <sub>5,45</sub> - 48 <sub>4,44</sub>	44.43	284.76
	329965.688	48 <sub>6,43</sub> - 47 <sub>5,42</sub>	42.45	282.71
	329965.688	48 <sub>5,43</sub> - 47 <sub>6,42</sub>	42.45	282.71
	329966.047	40 <sub>14,27</sub> - 39 <sub>13,26</sub>	27.08	251.42
	329966.047	40 <sub>13,27</sub> - 39 <sub>14,26</sub>	27.08	251.42
2	336125.535	54 <sub>1,54</sub> - 53 <sub>0,53</sub>	53.48	299.88
	336125.535	54 <sub>0,54</sub> - 53 <sub>1,53</sub>	53.48	299.88
	336127.005	43 <sub>12,32</sub> - 42 <sub>11,31</sub>	31.81	272.72
	336127.005	43 <sub>11,32</sub> - 42 <sub>12,31</sub>	31.81	272.72
	336127.169	44 <sub>10,34</sub> - 43 <sub>11,33</sub>	33.72	277.25
	336127.169	44 <sub>11,34</sub> - 43 <sub>10,33</sub>	33.72	277.25
	336127.422	42 <sub>12,30</sub> - 41 <sub>13,29</sub>	29.92	267.78
	336127.422	42 <sub>13,30</sub> - 41 <sub>12,29</sub>	29.92	267.78
	336127.563	53 <sub>2,52</sub> - 52 <sub>1,51</sub>	51.45	299.47
	336127.563	53 <sub>1,52</sub> - 52 <sub>2,51</sub>	51.45	299.47
	336127.680	45 <sub>10,36</sub> - 44 <sub>9,35</sub>	35.63	281.37
	336127.680	45 <sub>9,36</sub> - 44 <sub>10,35</sub>	35.63	281.37
	336128.356	46 <sub>8,38</sub> - 45 <sub>7,37</sub>	37.57	285.07
	336128.356	46 <sub>9,38</sub> - 45 <sub>8,37</sub>	37.57	285.07
	336128.740	41 <sub>14,28</sub> - 40 <sub>13,27</sub>	28.05	262.43
	336128.740	41 <sub>13,28</sub> - 40 <sub>14,27</sub>	28.05	262.43
	336128.946	52 <sub>3,50</sub> - 51 <sub>2,49</sub>	49.43	298.65
	336128.946	52 <sub>2,50</sub> - 51 <sub>3,49</sub>	49.43	298.65
	336129.052	47 <sub>8,40</sub> - 46 <sub>7,39</sub>	39.51	288.36
	336129.052	47 <sub>7,40</sub> - 46 <sub>8,39</sub>	39.51	288.36
	336129.643	48 <sub>6,42</sub> - 47 <sub>5,41</sub>	41.47	291.24
	336129.643	48 <sub>7,42</sub> - 47 <sub>6,41</sub>	41.47	291.24
	336129.762	51 <sub>3,48</sub> - 50 <sub>4,47</sub>	47.43	297.42
	336129.762	51 <sub>4,48</sub> - 50 <sub>3,47</sub>	47.43	297.42
	336130.023	49 <sub>6,44</sub> - 48 <sub>5,43</sub>	43.45	293.71
	336130.023	49 <sub>5,44</sub> - 48 <sub>6,43</sub>	43.45	293.71
	336130.092	50 <sub>5,46</sub> - 49 <sub>4,45</sub>	45.43	295.77
	336130.092	50 <sub>4,46</sub> - 49 <sub>5,45</sub>	45.43	295.77
	336131.417	40 <sub>15,26</sub> - 39 <sub>14,25</sub>	26.20	256.66
	336131.417	40 <sub>14,26</sub> - 39 <sub>15,25</sub>	26.20	256.66
3	338017.612	27 <sub>27,1</sub> - 26 <sub>26,0</sub>	24.97	146.26
	338018.346	27 <sub>27,0</sub> - 26 <sub>26,1</sub>	24.97	146.26

**Table 2.** (continued).

Line	Rest Frequency (MHz)	Transition $J_{K_a, K_c} - J_{K'_a, K'_c}$	$S_{ul}^*$	$E_l^\dagger$ ( $\text{cm}^{-1}$ )
4	342289.902	55 <sub>1,55</sub> - 54 <sub>0,54</sub>	54.48	311.09
	342289.902	55 <sub>0,55</sub> - 54 <sub>1,54</sub>	54.48	311.09
	342290.286	44 <sub>12,33</sub> - 43 <sub>11,32</sub>	32.80	283.93
	342290.286	44 <sub>11,33</sub> - 43 <sub>12,32</sub>	32.80	283.93
	342290.410	43 <sub>12,31</sub> - 42 <sub>13,30</sub>	30.91	278.99
	342290.410	43 <sub>13,31</sub> - 42 <sub>12,30</sub>	30.91	278.99
	342290.681	45 <sub>10,35</sub> - 44 <sub>11,34</sub>	34.70	288.46
	342290.681	45 <sub>11,35</sub> - 44 <sub>10,34</sub>	34.70	288.46
	342291.342	42 <sub>13,29</sub> - 41 <sub>14,28</sub>	29.03	273.64
	342291.342	42 <sub>14,29</sub> - 41 <sub>13,28</sub>	29.03	273.64
	342291.379	46 <sub>9,37</sub> - 45 <sub>10,36</sub>	36.62	292.58
	342291.379	46 <sub>10,37</sub> - 45 <sub>9,36</sub>	36.62	292.58
	342291.921	54 <sub>1,53</sub> - 53 <sub>2,52</sub>	52.45	310.68
	342291.921	54 <sub>2,53</sub> - 53 <sub>1,52</sub>	52.45	310.68
	342292.209	47 <sub>8,39</sub> - 46 <sub>9,38</sub>	38.56	296.28
	342292.209	47 <sub>9,39</sub> - 46 <sub>8,38</sub>	38.56	296.28
	342293.032	48 <sub>8,41</sub> - 47 <sub>7,40</sub>	40.51	299.58
	342293.032	48 <sub>7,41</sub> - 47 <sub>8,40</sub>	40.51	299.58
	342293.280	53 <sub>3,51</sub> - 52 <sub>2,50</sub>	50.43	309.86
	342293.280	53 <sub>2,51</sub> - 52 <sub>3,50</sub>	50.43	309.86
	342293.488	41 <sub>14,27</sub> - 40 <sub>15,26</sub>	27.17	267.87
	342293.488	41 <sub>15,27</sub> - 40 <sub>14,26</sub>	27.17	267.87
	342293.729	49 <sub>6,43</sub> - 48 <sub>7,42</sub>	42.47	302.46
	342293.729	49 <sub>7,43</sub> - 48 <sub>6,42</sub>	42.47	302.46
	342294.057	52 <sub>3,49</sub> - 51 <sub>4,48</sub>	48.43	308.63
	342294.057	52 <sub>4,49</sub> - 51 <sub>3,48</sub>	48.43	308.63
	342294.195	50 <sub>5,45</sub> - 49 <sub>6,44</sub>	44.44	304.93
	342294.195	50 <sub>6,45</sub> - 49 <sub>5,44</sub>	44.44	304.93
	342294.334	51 <sub>5,47</sub> - 50 <sub>4,46</sub>	46.43	306.98
	342294.334	51 <sub>4,47</sub> - 50 <sub>5,46</sub>	46.43	306.98
	342297.447	40 <sub>15,25</sub> - 39 <sub>16,24</sub>	25.33	261.70
	342297.447	40 <sub>16,25</sub> - 39 <sub>15,24</sub>	25.33	261.70
5	348453.267	44 <sub>12,32</sub> - 43 <sub>13,31</sub>	31.89	290.41
	348453.267	44 <sub>13,32</sub> - 43 <sub>12,31</sub>	31.89	290.41
	348453.422	45 <sub>12,34</sub> - 44 <sub>11,33</sub>	33.78	295.35
	348453.422	45 <sub>11,34</sub> - 44 <sub>12,33</sub>	33.78	295.35
	348453.838	43 <sub>14,30</sub> - 42 <sub>13,29</sub>	30.01	285.06
	348453.838	43 <sub>13,30</sub> - 42 <sub>14,29</sub>	30.01	285.06
	348454.040	46 <sub>11,36</sub> - 45 <sub>10,35</sub>	35.69	299.88
	348454.040	46 <sub>10,36</sub> - 45 <sub>11,35</sub>	35.69	299.88
	348454.101	56 <sub>1,56</sub> - 55 <sub>0,55</sub>	55.48	322.51
	348454.101	56 <sub>0,56</sub> - 55 <sub>1,55</sub>	55.48	322.51
	348454.919	47 <sub>10,38</sub> - 46 <sub>9,37</sub>	37.61	304.00
	348454.919	47 <sub>9,38</sub> - 46 <sub>10,37</sub>	37.61	304.00
	348455.498	42 <sub>14,28</sub> - 41 <sub>15,27</sub>	28.15	279.29
	348455.498	42 <sub>15,28</sub> - 41 <sub>14,27</sub>	28.15	279.29
	348455.899	48 <sub>9,40</sub> - 47 <sub>8,39</sub>	39.55	307.70
	348455.899	48 <sub>8,40</sub> - 47 <sub>9,39</sub>	39.55	307.70
	348456.112	55 <sub>2,54</sub> - 54 <sub>1,53</sub>	53.45	322.10
	348456.112	55 <sub>1,54</sub> - 54 <sub>2,53</sub>	53.45	322.10
	348456.848	49 <sub>8,42</sub> - 48 <sub>7,41</sub>	41.50	310.99
	348456.848	49 <sub>7,42</sub> - 48 <sub>8,41</sub>	41.50	310.99
	348457.447	54 <sub>2,52</sub> - 53 <sub>3,51</sub>	51.43	321.28
	348457.447	54 <sub>3,52</sub> - 53 <sub>2,51</sub>	51.43	321.28
	348457.650	50 <sub>6,44</sub> - 49 <sub>7,43</sub>	43.47	313.87
	348457.650	50 <sub>7,44</sub> - 49 <sub>6,43</sub>	43.47	313.87
	348458.186	53 <sub>3,50</sub> - 52 <sub>4,49</sub>	49.42	320.04
	348458.186	53 <sub>4,50</sub> - 52 <sub>3,49</sub>	49.42	320.04
	348458.202	51 <sub>5,46</sub> - 50 <sub>6,45</sub>	45.44	316.34
	348458.202	51 <sub>6,46</sub> - 50 <sub>5,45</sub>	45.44	316.34
	348458.410	52 <sub>4,48</sub> - 51 <sub>5,47</sub>	47.43	318.40
	348458.410	52 <sub>5,48</sub> - 51 <sub>4,47</sub>	47.43	318.40

**Table 2.** (continued).

Line	Rest Frequency (MHz)	Transition $J_{K_a, K_c} - J_{K'_a, K'_c}$	$S_{ul}^*$	$E_1^\dagger$ ( $\text{cm}^{-1}$ )
	348458.771	41 <sub>15,26</sub> - 40 <sub>16,25</sub>	26.30	273.12
	348458.771	41 <sub>16,26</sub> - 40 <sub>15,25</sub>	26.30	273.12
6	363098.770	29 <sub>29,1</sub> - 28 <sub>28,0</sub>	26.97	169.23
	363099.057	29 <sub>29,0</sub> - 28 <sub>28,1</sub>	26.97	169.23

\* Line Strength.

† Lower energy level.

The strongest lines arise from blends of many transitions in high-J bandheads. These bandheads become more compact and have more lines at higher frequencies. On the other hand, following Boltzmann population distribution, intensities of individual transitions forming the spectral blends, or *bands*, maximize at appreciably lower frequencies (henceforth the Boltzmann maxima) than the maxima apparent in the spectral profiles in Figure 1. At  $T_{rot} = 100$  K, for example, the strongest individual band line, i.e., the Boltzmann maximum, though not obvious in the spectrum (the middle panel of Figure 1), is near 195 GHz. Nevertheless, because at such frequencies the band compression effect becomes dominant and compensates for the intensity decrease of transitions at frequencies beyond the Boltzmann maximum, the overall band profile reaches an intensity maximum at the much higher frequency of  $\sim 300$  GHz. Similarly at  $T_{rot} = 50$  K and 200K, the Boltzmann maxima are at  $\sim 135$  GHz and  $\sim 285$  GHz, respectively, while at higher frequencies where band compression dominates, the *apparent* maximum intensity features for a linewidth of  $7 \text{ km s}^{-1}$  are predicted to be at  $\sim 180$  GHz and  $\sim 335$  GHz, accordingly. The 324 GHz spectral blend, which protrudes above the general profile and is seen in the middle and bottom panels of Figure 1, arises from accidental addition of some non-band lines to the spectral blend. The prevailing spectral features at 100 K and 200 K are compact high-J R-type bandheads of the type observed in our search (see Table 2). For an excitation temperature near 100 K, it is clear that searches in the spectral region near 1-mm (300 GHz) should provide the best chance for a detection.

### 3 RESULTS

Table 3 lists the important measured physical parameters of all the pyrimidine lines observed. The pyrimidine lines are separated into three sources according to the actual observations (Column 1). Column 2 gives the line numbers, which correspond to the line numbers shown in Column 1 of Table 2. Most of the pyrimidine lines are only observed in one or two sources but not in all. The fact that most of the data are fragmentary is mainly due to scheduling difficulties at the JCMT, leading to limited or uncertain availability of observing time for different sources.

In total, 6 different pyrimidine lines were observed toward the 3 target sources. The peak antenna temperature of the spectral line observed, i.e. the  $T_A^*$  upper limit for a non-detection, is given in Column 3 in mK; “rms” indicates the  $1-\sigma$  noise level per channel of the spectrum, where  $\sigma \equiv T_A^*(rms)$ .

Column 4 lists the upper limits of the total column density  $N_{tot}$  derived.  $T_A^*$ , hence also  $N_{tot}$ , are not listed if the target pyrimidine line is completely overwhelmed by nearby *strong* interlopers. Self-explanatory comments for each spectral line observed in each source are given, when necessary, in Column 5. Interlopers, which are largely blended with (denoted as “(B)”) and smeared out the target pyrimidine lines or partially blended (denoted as “(PB)”) with the candidate lines, are also included in Column 5 in the format *molecule/frequency(MHz)*.

Assuming that the pyrimidine lines are optically thin, in LTE, and that the rotational excitation temperature,  $T_{rot}$ , is much higher than the background brightness temperature, the beam-averaged total column density of  $c\text{-C}_4\text{H}_4\text{N}_2$  can be written as:

$$N_{tot}(\text{cm}^{-2}) = (1.669 \times 10^{17}) \frac{W_K Q_{rot}}{\nu} \left\{ \sum \left[ \frac{S_{ul} \mu_b^2}{\exp\left(\frac{E_u}{T_{rot}}\right)} \right] \right\}^{-1}, \quad (1)$$

where

$$W_K = \int T_R^* dv = \int \frac{T_A^*}{\eta_{fss}} dv \quad (2)$$

in ( $\text{K km s}^{-1}$ ) is the integrated intensity of the spectral *line* either from a single pyrimidine transition, or from unresolved multi-transitions such as in a bandhead. The rest frequency (MHz) is  $\nu$ ,  $\mu_b$  the permanent *b*-dipole moment in Debye,  $S_{ul}$  the line strength,  $E_u$  the upper energy level in K and  $Q_{rot}$  the rotational partition function. All pyrimidine lines reported here contain more than one pyrimidine transition, a summation of  $(S_{ul} \mu_b^2) / [\exp(E_u/T_{rot})]$  over all relevant transitions was thus applied. In addition, a rotational temperature  $T_{rot} = 100$  K was assumed for all transitions. In the case of a non-detection, for an interloper-blended pyrimidine line,  $T_R^*$  is obtained from the  $T_A^*$  upper limit listed in Column 3 of Table 3 corrected for  $\eta_{fss}$ . If the equivalent linewidth could not be unambiguously defined from the observed spectrum, the column density limits were evaluated using a representative value of the equivalent linewidth; a value of  $\Delta v \simeq 10 \text{ km s}^{-1}$  was adopted for all three target sources.

Sample pyrimidine spectra are shown in Figures 2 and 3. With a limited number of spectral lines observed in each source, our submillimeter-wave search for pyrimidine did not yield a definite detection of pyrimidine in either Sgr B2(N) or Orion KL. By averaging over all observed lines measurable in each source (see Table 3), the inferred upper limits on the total column density in Sgr B2 and Orion are  $1.7 \times 10^{14} \text{ cm}^{-2}$  and  $2.4 \times 10^{14} \text{ cm}^{-2}$ , respectively.

In the case of W51 e1/e2, there is a spectral feature at  $\sim 57 \text{ km s}^{-1}$  with respect to the rest frequency adopted for the observation (see the spectrum shown in the lower panel of Figure 3). This feature coincides precisely with the  $J \leq 55$  band-head of pyrimidine between 342289.9 and 342297.4 MHz (Line 4), containing 32 transitions at  $V_{LSR} = 59.0 \text{ km s}^{-1}$ . An unidentified U-line at 342290.0 MHz was previously reported in a line survey of Orion KL (Schilke, et al. 1997); unfortunately we did not observe either Orion or Sgr B2 at this particular frequency.

The total pyrimidine column density in W51 e1/e2 derived solely from Line 4 is  $4.8 \times 10^{14} \text{ cm}^{-2}$ ; the averaged upper limit to the column density from all 3 lines available in

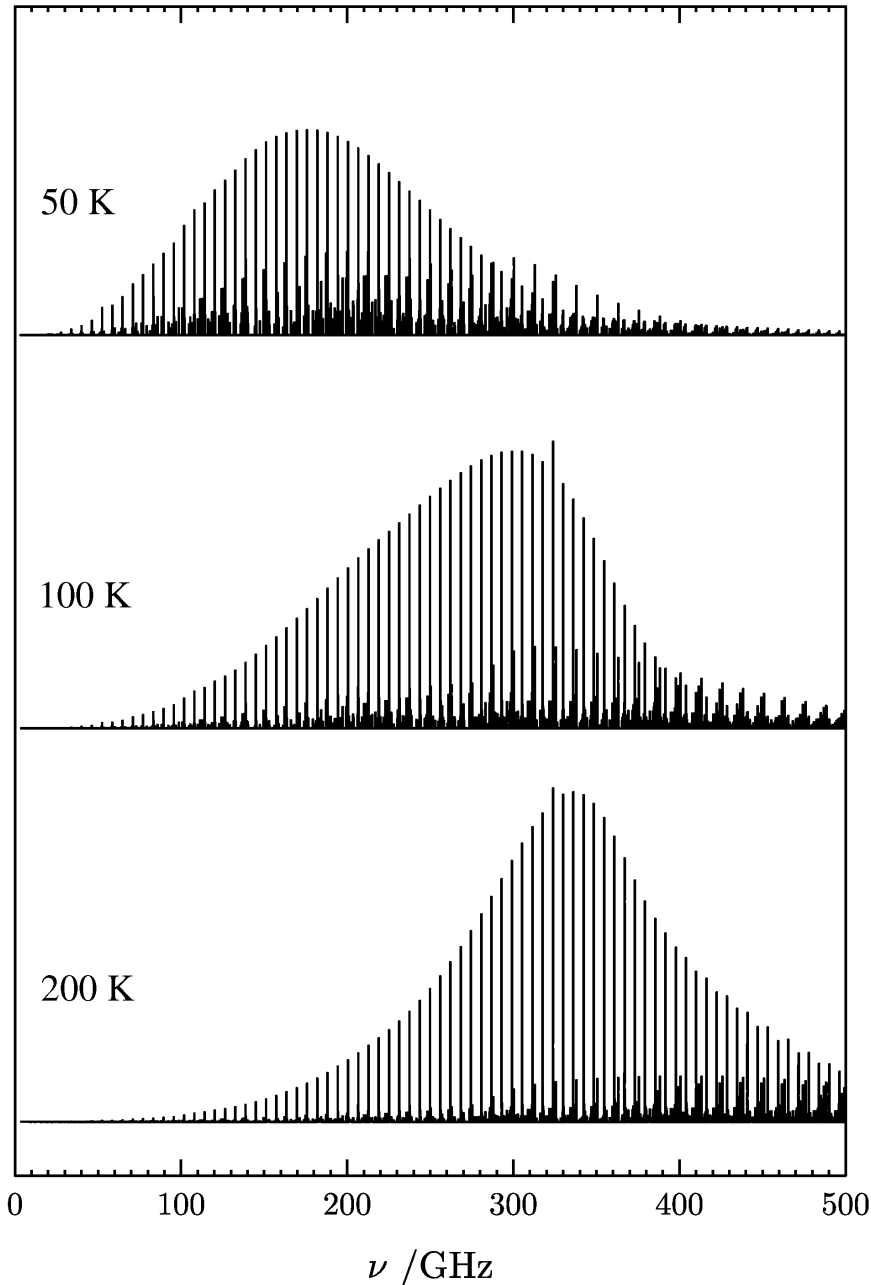


**Figure 1.** The predicted relative line intensity of the pyrimidine spectra over a frequency range of 0 to 500 GHz at various excitation temperatures (50 K, top; 100 K, middle; and 200 K, bottom). The ordinate is in an arbitrary scale. These spectra are actually contour plots with point spacing of 0.5 MHz but have the appearance of stick diagrams because line contours are very narrow relative to the total breadth of the plotted spectrum. Each such stick is thus in fact a very compressed line profile for a spectral blend, and each spectrum is in principle 1000000 points long. The simulation is for a Gaussian lineshape with an assumed equivalent linewidth (FWHM) of 7 km s<sup>-1</sup>. The *apparent* maximum intensity features are at ~180 GHz for 50 K, ~300 GHz for 100 K and ~335 GHz for 200 K. The 324 GHz spectral peak (middle & bottom) is due to accidental addition of some non-band lines to the spectral blend.

W51 is  $N_{tot} \leq 3.4 \times 10^{14}$  cm<sup>-2</sup>. It is interesting to note that the pyrimidine column density computed only from Line 4 (assuming  $T_{rot} = 100$  K) is just slightly higher (within a factor of 2) than the upper limits deduced from the two other, interloper-contaminated, lines. It appears that if Line 4 of W51 is truly a detection, we may have expected to detect another bandhead, Line 5, whose transitions are at higher frequencies. It could be argued that the fact that we failed to detect Line 5 makes the identification of Line 4 less likely.

However, Line 5 is expected to be much weaker than Line 4 at an excitation temperature lower than 100 K, and so, in the absence of accurately measured pyrimidine rotational temperatures for these sources, we cannot entirely rule out a true detection in W51.

Finally, the submillimeter transitions targeted in this search possess rather high excitation levels, and so any observable pyrimidine emission would mostly originate from regions of high temperature and/or density, if radiative ex-

**Table 3.** The measured physical parameters of the pyrimidine lines observed.

Source	Line	$T_A^* \pm \text{rms}$ (mK)	$N_{tot}$ ( $10^{14} \text{ cm}^{-2}$ )	Comment
Sgr B2(N)	1	—	—	(B) C <sub>2</sub> H <sub>5</sub> OH/329954.9; (B) C <sub>2</sub> H <sub>5</sub> OH/329956.5; (B) C <sub>2</sub> H <sub>5</sub> OH/329968.2
Sgr B2(N)	3	52.6±13.5	<1.68	(B) CH <sub>3</sub> OCH <sub>3</sub> /338025.5
Sgr B2(N)	5	—	—	(B) CH <sub>3</sub> CHO/348449.6; (B) C <sub>2</sub> H <sub>5</sub> CN/348473
Orion KL	2	215.7±13.8	<1.18	(B) <i>c</i> -C <sub>3</sub> H <sub>2</sub> /336128.5; (B) C <sub>2</sub> H <sub>3</sub> CN/336137.8; (PB) HCOOCH <sub>3</sub> /336111.3; (PB) SO <sub>2</sub> /336113.5
Orion KL	5	400.0±12.6	<3.66	contaminated by a spectral feature from the image sideband
Orion KL	6	—	—	(B) CH <sub>3</sub> C <sub>3</sub> N/363097.1; (B) Si <sup>18</sup> O/363100.7; (B) C <sub>2</sub> H <sub>5</sub> CN/363107
W51 e1/e2	3	140.6±12.9	<3.14	(B) CH <sub>3</sub> OCH <sub>3</sub> /338025.5
W51 e1/e2	4	631.3±23.6	<4.79	detected? (U-342290); (PB) C <sub>2</sub> H <sub>3</sub> CN/342286.8
W51 e1/e2	5	127.5±12.3	<2.20	(B) CH <sub>3</sub> CHO/348449.6

citation is negligible. As a result, these excited pyrimidine molecules would have been located in regions fairly close to protostellar hot cores within molecular clouds. It is therefore probable that the real source size is smaller than the telescope beam ( $\sim 14''$ ); it is more likely to be the case particularly for distant sources such as Sgr B2(N) and W51 e1/e2. Hence, one should note that our observations would suffer from beam dilution if the source extent is indeed smaller than the beam. The derived upper limits on the column densities, based on the assumption that the source fills the beam, could consequently be underestimated.

The upper limits of fractional abundance of pyrimidine with respect to molecular hydrogen,  $X(c-C_4H_4N_2) = N_{tot}(c-C_4H_4N_2)/N_{tot}(H_2)$ , may also be deduced. Molecular hydrogen column densities inferred from single-dish observations with beam sizes similar to the JCMT are employed, in order to determine the beam-averaged abundances more accurately. The H<sub>2</sub> column densities adopted are:  $\simeq 5 \times 10^{24} \text{ cm}^{-2}$  for Sgr B2(N) (Nummelin et al. 2000),  $8 \times 10^{23} \text{ cm}^{-2}$  for Orion KL (Sutton et al. 1995), and  $1 \times 10^{24} \text{ cm}^{-2}$  for W51 e1/e2 (Jaffe, Becklin & Hildebrand 1984). The upper limits of pyrimidine fractional abundances thus estimated are  $X(c-C_4H_4N_2) \leq 3.4 \times 10^{-11}$  for Sgr B2,  $3.0 \times 10^{-10}$  for Orion, and  $3.4 \times 10^{-10}$  for W51.

#### 4 DISCUSSION

Our submillimeter search for the nucleic acid building-block pyrimidine has not been successful. We have perhaps detected one *line* in a single source but this needs to be confirmed. The negative result therefore cannot be considered definitive and searches at lower frequencies may yet detect pyrimidine in hot cores. The low inferred pyrimidine abundance limits may simply reflect the fact that pyrimidine is generally of low abundance in massive star-forming cores, and hence it is difficult to populate the high-J energy levels ( $J \leq 56$  in our study) which are observable at submillimeter wavelengths. On the other hand, it could also imply that either pyrimidine is not evaporated efficiently from dust grains at hot core temperatures, or is destroyed easily in the warmest regions in hot cores sampled by submillimeter observations.

It would appear that the best chance for an astronom-

ical detection of pyrimidine, and other Nitrogen Heterocycles, is probably in the circumstellar envelopes (CSEs) of carbon stars. AGB and post-AGB stars (e.g. IRC+10216, CRL 618 and CRL 2688) are copious producers of carbonaceous dust particles. Recent ISO observations of well-known protoplanetary nebulae (PPNe) have uncovered more new organic molecules, including the first detection of benzene in CRL 618 (Cernicharo et al. 2001a, 2001b). The initial stages of dust formation involve polymerization of acetylene to form benzene and subsequent C<sub>2</sub>H<sub>2</sub> additions lead to large polycyclic aromatic hydrocarbon (PAH) molecules (e.g. Cherchneff, Barker & Tielens 1992). During this reaction sequence other triply-bonded molecules can also add to the growing ring structures. In particular, recent theoretical work indicates that N atoms can become incorporated in ring structures through additions involving HCN (Ricci, Bauschlicher & Bakes 2001). However, the kinetics of ring growth suggests that single rings containing two N atoms will be less favoured than single rings with one N atom (i.e. pyridine). Even two-ring compounds containing a single N atom, such as quinoline and isoquinoline, the N-substituted analogues of naphthalene, could be more abundant than pyrimidine (Kisiel et al. 2003) and may explain why our search appears to have been unsuccessful. Searches for pyridine, quinoline and isoquinoline in the molecular envelopes of evolved stars are currently underway.

As an alternative to ring formation in neutral-neutral reactions, Woods, et al. (2002) have shown that ion-molecule reactions are able to account for the abundance of benzene observed in CRL 618. The growth of larger rings, and incorporation of heteroatoms into them, has not yet been considered in circumstellar ion-molecule chemistry. Woods, et al. (2003) have proposed one neutral process, involving benzene and CN, that could lead to nitrogen being added to ring structures. However, the product of this reaction has the nitrogen present in a side-group (i.e. benzonitrile, *c*-C<sub>6</sub>H<sub>5</sub>CN) and not bonded into the ring.

Another possible reason for a low interstellar pyrimidine abundance concerns its photostability. The infrared spectra and photostability of pyrimidine have recently been measured in an Ar matrix at 10 K (Peeter et al. 2003). The stability of pyrimidine (which does not have real aromatic properties) against UV photolysis is rather limited and far below that of mono and polycyclic aromatic rings. These ex-

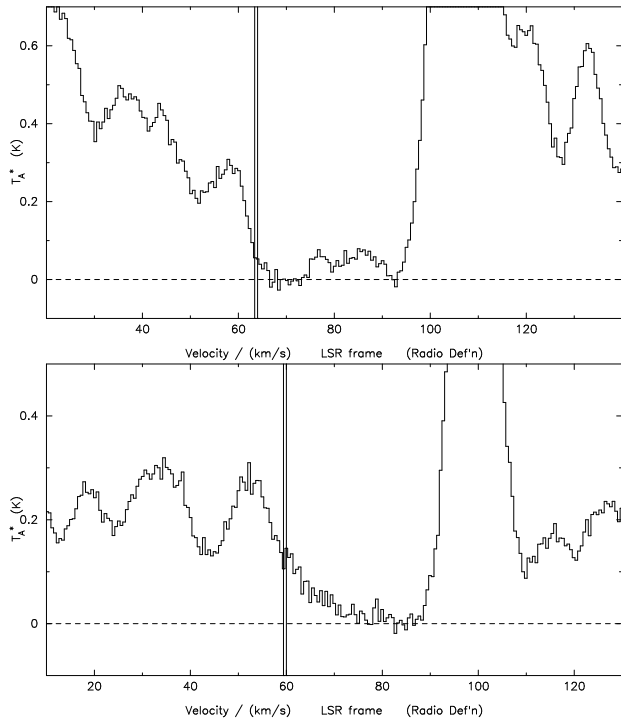


**Figure 2.** Sample pyrimidine spectra at 338.0 GHz (Line 3; 2727,1-2626,0 and 2727,0-2626,1) of Sgr B2(N) (top) and of W51 e1/e2 (bottom). The two vertical lines mark the two expected transitions of pyrimidine. The abscissae give the LSR velocities with respect to the rest frequencies adopted for the observations at the nominal LSR velocities  $64.0 \text{ km s}^{-1}$  for Sgr B2(N) and  $60.0 \text{ km s}^{-1}$  for W51 e1/e2.

periments appear to indicate that any circumstellar pyrimidine would be easily destroyed by UV photons, or cosmic ray particles, soon after delivery to the interstellar medium. In this case, any interstellar pyrimidine would have to be produced in dark molecular clouds.

## 5 CONCLUSION

To strengthen the role of prebiotic interstellar matter in Astrobiology, we have searched for 6 pyrimidine lines in three massive star-forming regions: Sgr B2(N), Orion KL and W51 e1/e2. Our search was unsuccessful and did not yield a conclusive result, with only one potential single-line detection. The abundance limits inferred are  $\leq 3.4 \times 10^{-11}$  for Sgr B2,  $3.0 \times 10^{-10}$  for Orion, and  $3.4 \times 10^{-10}$  for W51. Our negative result may simply reflect the fact that interstellar pyrimidine is of low abundance. Sources that are ongoing sites of carbon dust formation, such as the C-rich envelopes of AGB and post-AGB stars, probably present the best opportunity for detecting pyrimidine and other nitrogen heterocycles.

## 6 ACKNOWLEDGEMENTS

We would like to thank the referee, Tom J. Millar, for his useful comments and suggestions. The research of YJK was

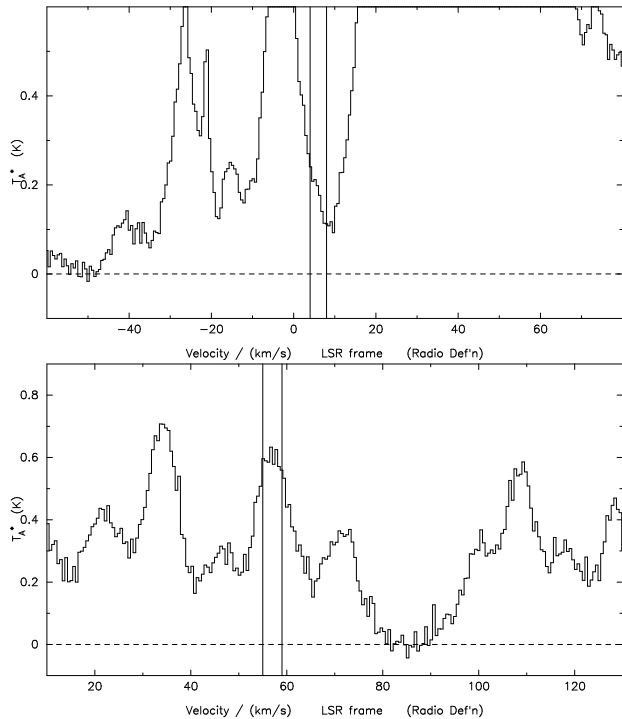


**Figure 3.** Sample pyrimidine spectra at the 336.1 GHz band head (Line 2; with  $J \leq 54$ ) of Orion KL (top), and at the 342.3 GHz band head (Line 4; with  $J \leq 55$ ) of W51 e1/e2 (bottom). The two verticals enclose the 336.1 GHz band head (top) and the 342 GHz band head (bottom). A tentative detection of pyrimidine in W51 e1/e2 is visible in the bottom panel. The assumed LSR velocities for the rest frequencies adopted for the observations are  $8.0$  and  $60.0 \text{ km s}^{-1}$  for Orion KL and W51 e1/e2, respectively.

supported by NSC grants 90-2112-M-003-012 and 91-2112-M-003-016. This work was supported by NASA's Exobiology Program, through NASA Ames Interchange NCC2-1162, and by the Netherlands Research School for Astronomy (NOVA). We wish to thank Remo P.J. Tilanus for his kind support and help while observing at the JCMT.

## REFERENCES

- Allamandola L.J., Bernstein M.P., Sandford S.A., 1997, in Cosmovici C.B., Bowyer S., Wertheimer D., eds, *Astronomical & Biochemical Origins and the Search for Life in the Universe*, Bologna: Editrice Compositori, p.23
- Blake G.A., Sutton E.C., Masson C.R., Phillips T.G., 1987, *ApJ*, 315, 621
- Cernicharo J., Heras A.M., Tielens A.G.G.M., Pardo J.R., Herpin F., Guélin M., Waters L.B.F.M., 2001a, *ApJL*, 546, L123
- Cernicharo J., Heras A.M., Pardo J.R., Tielens A.G.G.M., Guélin M., Dartois E., Neri R., Waters L.B.F.M., 2001b, *ApJL*, 546, L127
- Charnley S.B., Ehrenfreund P., Kuan Y.-J., 2001, *Spectrochimica Acta*, 57, 685
- Cherchneff I., Barker J.R., Tielens A.G.G.M., 1992, *ApJ*, 401, 269
- Chyba C.F., Thomas P.J., Brookshaw L., Sagan C., 1990, *Sci*, 249, 366

- Dickens J.E., Irvine W.M., Ohishi M., Ikeda M., Ishikawa S., Nummelin A., Hjalmarson Å., 1997, *ApJ*, 489, 753
- Dickens J.E., Irvine W.M., Nummelin A., Mollendal H., Saito S., Thorwirth S., Hjalmarson Aa., Ohishi M., 2001, *Spectrochimica Acta*, 57, 643
- Ehrenfreund, P. and Charnley, S.B., 2000, *ARA&A*, 38, 429
- Ehrenfreund P., Irvine W., Becker L., et al., 2002, *Reports on Progress in Physics*, 65, 10, 1427
- Greenberg J.M., Gillette J.S., Muñoz Caro G.M., Mahajan T.B., Zare R.N., Li A., Schutte W.A., de Groot M., & Mendoza-Gómez C., 2000, *ApJ*, 531, 71
- Hollis J.M., Lovas F.J., Jewell P.R., 2000, *ApJ*, 540, L107
- Irvine W.M., Ellder J., Hjalmarson Å., Kollberg E., Rydbeck O.E.H., Sorensen G.O., Bak B., Svanholt H., 1981, *A&A*, 97, 192
- Jaffe D.T., Becklin E.E., Hildebrand R.H., 1984, *ApJL*, 279, L51
- Kisiel Z., Pszczółkowski L., López J.C., Alonso J.L., Maris A., Caminati W., 1999, *J. Mol. Spectrosc.*, 195, 332
- Kisiel Z., Desyatnyk O., Pszczółkowski L., Charnley S.B., Ehrenfreund P., 2003, *J. Mol. Spectrosc.*, 217, 115
- Krueger F.R., Korth A., Kissel J., 1991, *Space Sci. Rev.*, 56, 167
- Kuan Y.-J., Charnley S.B., Huang H.-C., Tseng W.-L., Kisiel, Z., 2003, tp appear in the August 20 issue of *ApJ*
- Kuan Y.-J., Huang H.-C., Charnley S.B., Snyder L.E., Wilson T.L., Bohn R.K., Ohishi M., Lovas F.J., Butner H.M., Thorwirth S., 2003, in Celnikier, L.M., Tran Thanh Van, J., eds, the proceedings of the XIIth Rencontres de Blois on Frontiers of Life, The Gioi, Vietnam, p.257
- Miao Y., Mehringer D.M., Kuan Y.-J., Snyder L.E., 1995, *ApJ*, 445, L59
- Myers P.C., Thaddeus P., Linke R.A., 1980, *ApJ*, 241, 155
- Nummelin A., Dickens J.E., Bergman P., Hjalmarson Å., Irvine W.M., Ikeda M., Ohishi M., 1998, *A&A*, 337, 275
- Nummelin A., Bergman P., 1999, *A&A*, 341, L59
- Nummelin A., Bergman P., Hjalmarson Å., Friberg P., Irvine W.M., Millar T.J., Ohishi M., Saito S., 2000, *ApJS*, 128, 213
- Peeter Z., et al., 2003, *A&A*, submitted
- Remijan A.J., Snyder L.E., Liu S.-Y., Mehringer D., Kuan Y.-J., 2002, *ApJ*, 576, 264
- Ricci A., Bauschlicher C.W., Bakes E.L.O., 2001, *Icarus*, 154, 516
- Schilke P., Groesbeck T.D., Blake G.A., Phillips T.G., 1997, *ApJS*, 108, 301
- Simon M.N., Simon M., 1973, *ApJ*, 184, 757
- Stoks P.G., Schwartz A.W., 1981, *Geochim. Cosmochim. Acta*, 45, 563
- Stoks P.G., Schwartz A.W., 1982, *Geochim. Cosmochim. Acta*, 46, 309
- Sutton E.C., Peng R., Danchi W.C., Jaminet P.A., Sandell G., Russell A.P.G., 1995, *ApJS*, 97, 455
- Turner B.E., 1991, *ApJS*, 76, 617
- Woods P.M., Millar T.J., Zijlstra A.A., Herbst E., 2002, *ApJL*, 574, L167
- Woods P.M., Millar T.J., Herbst E., Zijlstra A.A., 2003, *A&A*, 402, 189
- Ziurys L.M., Turner B.E., 1986, *ApJL*, 300, L19